Eur. J. Mineral., 35, 969–985, 2023
https://doi.org/10.5194/ejm-35-969-2023

European Journal of Mineralogy
Open Access

Symplectite and kelyphite formation during decompression of mafic granulite from Gjelsvikfjella, central Dronning Maud Land, Antarctica

Synnøve Elvevold[1], Joachim Jacobs[2], Leif-Erik Rydland Pedersen[2], Øyvind Sunde[1], Ane K. Engvik[3], and Per Inge Myhre[1]

[1]Norwegian Polar Institute, P.O. Box 6606 Stakkevollan, 9296 Tromsø, Norway
[2]Department of Earth Science, University of Bergen, P.O. Box 7803, 5020 Bergen, Norway
[3]Geological Survey of Norway, P.O. Box 6315 Torgarden, 7491 Trondheim, Norway

Correspondence: Synnøve Elvevold (elvevold@npolar.no)

Received: 31 March 2023 – Revised: 15 September 2023 – Accepted: 25 September 2023 – Published: 14 November 2023

Abstract. Central Dronning Maud Land (cDML) is part of the late Mesoproterozoic Maud Belt in East Antarctica, which was metamorphosed and deformed during the Ediacaran–Cambrian Gondwana assembly. Here we study high-pressure (HP) mafic rocks in Gjelsvikfjella, cDML, which occur as lenses and pods transposed in highly strained, upper amphibolite-facies gneisses. We present a P–T–t history for the HP rocks based on mineral assemblages, reaction textures and new U–Pb zircon data. Relics that indicate an early HP granulite-facies stage have been identified in anhydrous garnet–clinopyroxene rocks. The peak-pressure assemblage was plagioclase-free and contained garnet, titanite, clinopyroxene and quartz. The HP assemblage has been extensively overprinted by lower-pressure phases and exhibits a variety of symplectite and corona textures that record the post-peak-pressure evolution of the rocks. Decompression and heating in the granulite-facies field resulted in the replacement of titanite by ilmenite–clinopyroxene symplectite, formation of clinopyroxene–plagioclase intergrowths and resorption of garnet by plagioclase–clinopyroxene kelyphite. Formation of late orthopyroxene in symplectites and kelyphites demonstrates that the P–T evolution entered the medium-pressure granulite-facies field. The peak metamorphic stage was followed by retrograde cooling into the amphibolite facies. In situ laser ablation inductively coupled plasma mass spectrometry (LA-ICP-MS) U–Pb dating of zircons indicate Mesoproterozoic protolith ages (1150–1000 Ma) and Ediacaran–Cambrian metamorphic reworking at ca. 568 and ca. 514 Ma. The HP granulites were formed and exhumed during a clockwise P–T evolution related to continental collision during Gondwana amalgamation, followed by post-collisional extension and orogenic collapse.

1 Introduction

Symplectite is a textural term that refers to an intimate, commonly lamellar, vermicular (worm-like) or globular intergrowth of two or more phases (Passchier and Trouw, 1998). The intergrowth may form by reaction between adjacent phases or by decomposition of a single phase; the latter is usually referred to as exsolution symplectite. Kelyphite is a specific type of symplectite that replaces and forms a corona surrounding garnet and which may consist of several phases such as plagioclase, pyroxene, spinel and/or amphibole (e.g., Carswell et al., 1996; Passchier and Trouw, 1998). Symplectite and kelyphite are common features in high-pressure (HP) mafic rocks that have experienced decompression during exhumation to shallower crustal levels. For instance, a characteristic reaction texture in retrogressed eclogite is lamellar intergrowth of Ca-clinopyroxene + plagioclase after omphacite (e.g., Boland and Van Roermund, 1983; Carswell, 1990, and references therein; Joanny et al., 1991; Anderson and Moecher, 2007). Likewise, amphibolite- and granulite-facies mafic rocks, which contain reaction

rims of plagioclase + pyroxene ± amphibole after garnet, have commonly been considered evidence of former HP metamorphism (e.g., Joanny et al., 1991; Carswell et al., 1996).

Symplectite and corona textures, which reflect sluggish reaction kinetics, slow diffusion rates, and variations in the availability of fluid or intensity of deformation, are extremely useful in the determination of mineral reactions and segments of the P–T path followed by the host rocks (e.g., Elvevold and Gilotti, 2000; Sartini-Rideout et al., 2007). While fully equilibrated mineral assemblages only record a point in P–T space, partially equilibrated rocks can record major parts of their metamorphic evolution. A wide range of disequilibrium textures, such as compositional zoning, exsolution, symplectite, kelyphite, corona and reaction rims, can form during unloading to lower crustal levels and provide information on the shape of the decompressional P–T path (e.g., Cox and Indares, 1999).

Eclogite and HP granulite in collisional orogenic belts can provide important constraints on the tectonic evolution of the unit in which they occur. In this contribution, we describe complex symplectite and kelyphite in high-grade mafic rocks from Gjelsvikfjella, central Dronning Maud Land (cDML), East Antarctica. The reaction textures, which are preserved in the cores of competent, anhydrous mafic pods and lenses within orthogneisses, include unusual, vermicular symplectite of ilmenite + clinopyroxene, as well as globular intergrowths of plagioclase + clinopyroxene. Garnet is surrounded and replaced by kelyphite of plagioclase ± clinopyroxene ± orthopyroxene. The symplectitic breakdown textures indicate decompression from an early HP granulite-facies metamorphic stage. The mafic pods and the host orthogneiss share the same metamorphic P–T history, but they provide information on different parts of the P–T path. For kinetic and equilibrium reasons, mafic rocks tend to preserve HP assemblages relative to the non-mafic rocks (e.g., Koon and Thompson, 1985; Proyer, 2003). The metamorphic evolution of anatectic metapelitic gneiss and orthogneiss is characterized by medium-P assemblages (Bisnath and Frimmel, 2005; Engvik et al., 2007; Elvevold et al., 2020). Peak metamorphism reached granulite-facies conditions ($T \geq 810$–$830\,^{\circ}\mathrm{C}$) at mid-crustal levels.

We present the first in situ U–Pb laser ablation inductively coupled plasma mass spectrometry (LA-ICP-MS) analyses of zircons from cDML. Cathode luminescence (CL) imaging of zircon populations suggests more than one crystallization phase, indicating a complex growth–recrystallization history that is preserved in individual samples of the mafic enclaves. The combined metamorphic petrology and geochronology is used to infer a P–T–t path of the area and adds to the data and discussions provided by previous studies of the Maud Belt (e.g., Pauly et al., 2016).

2 Geological background

Recognizing HP metamorphic rocks in East Antarctica is important because these rocks can identify paleo-suture zones and constrain the age of collision events. HP–ultra-HP (UHP) metamorphism has been observed around the Antarctic craton in various orogenic belts (Godard and Palmeri, 2013), even though most of the continent is covered in ice. The Mesoproterozoic and late Neoproterozoic to early Paleozoic orogenic belts in East Antarctica are characterized by high-grade ortho- and paragneiss, migmatite, and granulite. Occurrences of eclogites and HP granulite-facies rocks have been reported from a few localities (e.g., Grew et al., 1989; Board et al., 2005; Schmädicke and Will, 2006).

The mountain range of Dronning Maud Land (DML) is exposed in a row of nunataks that are roughly parallel to the edge of the East Antarctic ice sheet, about 100–250 km inland. The geology of the western and central part of DML is separated into four main geological provinces (Fig. 1): (i) the Grunehogna Craton, (ii) Mesoproterozoic Natal-type orogenic crust, (iii) the Mesoproterozoic Maud Belt and (iv) the Tonian Oceanic Arc Super Terrane (TOAST). The Grunehogna Craton represents an Archean fragment of the Proto-Kalahari Craton (Groenewald et al., 1995), which experienced substantial crustal growth during the Mesoproterozoic (Jacobs et al., 2008). South of the Grunehogna Craton, Natal-type orogenic crust is exposed in the western Heimefrontfjella. The Grunehogna Craton and the Natal-type crust lack later Neoproterozoic to early Paleozoic reworking and are together interpreted as the western foreland of the East African–Antarctic Orogen (EAAO). The Maud Belt (1170–1030 Ma) is a high-grade orogenic belt related to the assembly of the supercontinent Rodinia (Jacobs et al., 1998, 2003a; Paulsson and Austrheim, 2003; Bisnath et al., 2006; Baba et al., 2015; Wang et al., 2020b) and shows pervasive and polyphase Neoproterozoic to early Paleozoic high-grade reworking. The Maud Belt forms the western part of the EAAO and stretches from Heimefrontfjella in the west, through Kirwanveggen, H.U. Sverdrupfjella, Gjelsvikfjella, Mühlig-Hofmannfjella, Orvinfjella to Wohlthatmassivet in the east (Figs. 1b, 2a). The eastern extent of the Maud Belt coincides with the Forster Magnetic Anomaly (Riedel et al., 2013), which is inferred as a significant tectonic boundary (Fig. 1b). Jacobs et al. (2015) interpreted the anomaly to represent a suture of the eastern margin of the Kalahari Craton and TOAST. The latter is characterized by 1000–900 Ma juvenile oceanic arcs, interpreted as remnants of the Mozambique Ocean that were accreted onto the Kalahari during Gondwana assembly. The TOAST also underwent strong late Neoproterozoic to early Paleozoic reworking and represents the eastern part of the EAAO (Jacobs et al., 2015).

The study area, close to the Norwegian research station Troll (Fig. 2b), lies within the Mesoproterozoic Maud Belt that formed through continental arc magmatism along

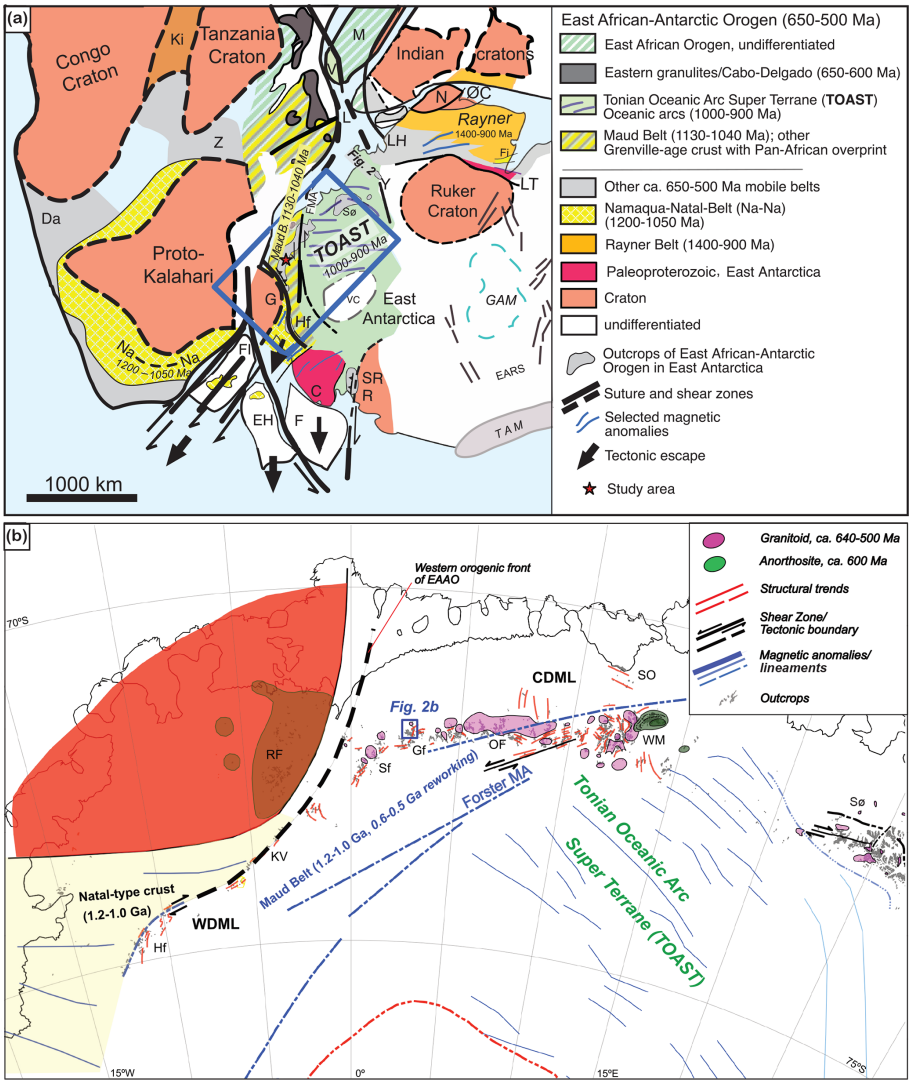

Figure 1. Location of the study area in a reconstruction of Gondwana and the East African–Antarctic Orogen **(a)** and Dronning Maud Land **(b)** (after Jacobs et al., 2015, 2020). The study area is located in the easternmost part of the Kalahari Craton. East Antarctica is shown in polar stereographic projection, whereas the adjacent continents are shown schematically. Abbreviations: C – Coats Land, CDML – central Dronning Maud Land, Da – Damara Belt, EARS – East Antarctic Rift System, EH – Ellsworth–Haag, F – Filchner block, FI – Falkland Islands, Fi – Fisher Terrane, FMA – Forster Magnetic Anomaly (abbreviated as Forster MA in panel b), G – Grunehogna, GAM – Gamburtsev Mountains, Gf – Gjelsvikfjella, Hf – Heimefrontfjella, KV – Kirwanveggen, Ki – Kibaran, L – Lurio Belt, LH – Lützow-Holm Bay, LT – Lambert Terrane, N – Napier Complex, Na – Namaqua-Natal, M – Madagascar, ØC – Øygarden Complex, R – Read Block, RF – Ritscherflya, Sf – H.U. Sverdrupfjella, OF – Orvinfjella, SO – Schirmacheroasen, Sø – Sør Rondane, SR – Shackleton Range, TAM – Transantarctic Mountains, V – Vohibori, VC – Valkyrie Craton, WM – Wohlthatmassivet, WDML – western Dronning Maud Land, Y – Yamato Mountains, Z – Zambezi Belt.

the eastern margin of the Kalahari Craton (e.g., Wang et al., 2020b). Arc magmatism was followed by intrusion of granitic plutons and felsic sheets accompanied by high-grade metamorphism around 1080–1030 Ma. The Maud Belt experienced intense reworking related to the Ediacaran–Cambrian (600–500 Ma) East African–Antarctic Orogen, which formed during the assembly of Gondwana (Jacobs et al., 1998, 2003b; Paulsson and Austrheim, 2003; Baba et al., 2015; Wang et al., 2020a; Elvevold et al., 2020). The Ediacaran–Cambrian event is commonly referred to as the Pan-African orogeny (Kennedy, 1964). The metamorphic rocks in cDML display a strong, high-grade Pan-African overprint, although late Mesoproterozoic protolith ages, as well as metamorphic ages, between 1.2 and 1.0 Ga are reported (Jacobs et al., 1998; Paulsson and Austrheim, 2003; Bisnath et al., 2006; Wang et al., 2020b). The metamorphic complex includes gneisses and migmatites of various composition and typically contains amphibolite-

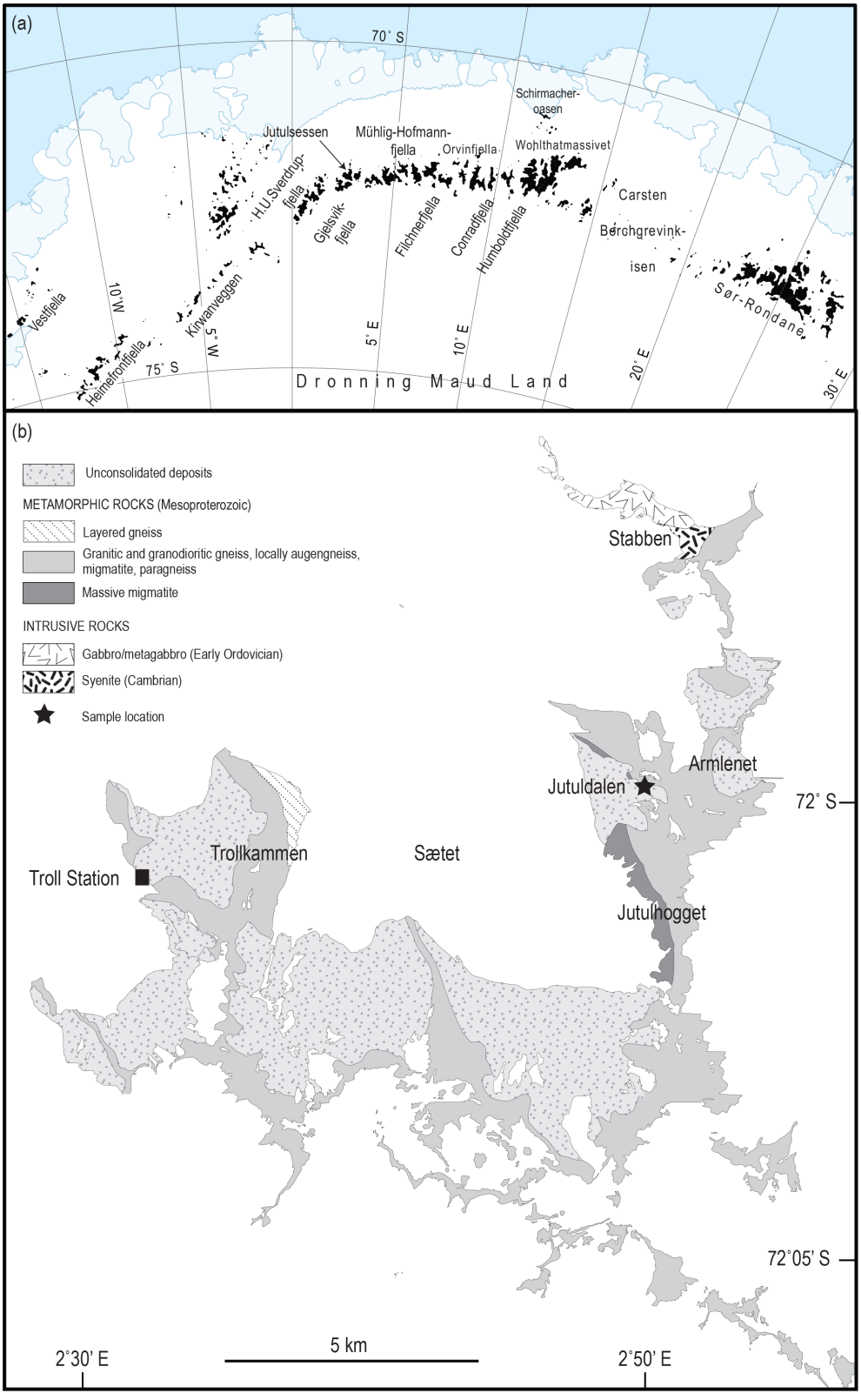

Figure 2. (a) Overview map of central Dronning Maud Land with place names. **(b)** Geological map of Jutulsessen, Gjelsvikfjella. Simplified after Elvevold et al. (2021).

and granulite-facies mineralogy. The onset of the high-grade overprint is loosely dated to 590–560 Ma (e.g., Jacobs et al., 1998, 2003b; Pauly et al., 2016; Elvevold et al., 2020). The gneisses record a clockwise P–T evolution characterized by a decompression segment followed by isobaric cooling (Elvevold and Engvik, 2013; Palmeri et al., 2018; Elvevold et al., 2020). The metamorphic complex is intruded by voluminous granitoid rocks at a late stage of the Pan-African orogeny. The granitoids are generally undeformed and include granitic, syenitic and monzonitic compositions. Some of the granitoids are characterized by Fe-enriched bulk compositions and contain fayalite or enstatite. The igneous suite in cDML intruded between 540–500 Ma (Mikhalsky et al., 1997; Paulsson and Austrheim, 2003; Jacobs et al., 2003b, 2008; Wang et al., 2020a). In the close-by Schirmacheroasen, an early Pan-African ultrahigh-temperature event is recorded between ca. 640–600 Ma, which has been interpreted in different ways but may relate to the back-arc extension of a retreating accretionary orogen prior to continental collision (Baba et al., 2010; Jacobs et al., 2020). The mafic rocks in this study are exposed in the Jutulsessen nunatak in Gjelsvikfjella (Fig. 2) and are present as lenses and disrupted layers in highly strained orthogneiss (Fig. 3a). The lenses, typically < 5 m in length and < 1 m in width, are composed of massive garnet amphibolite (Fig. 3b), garnet–clinopyroxene granulite (Fig. 3c) and amphibolite. The garnet–clinopyroxene granulites comprise an anhydrous mineral assemblage in the core and typically display retrogressed, hydrated margins consisting of amphibolite. The mafic rocks were originally dikes or mafic xenoliths in a calc-alkaline arc. Post-tectonic, felsic veins and dikes intrude the mafic pods, as well as the host biotite–gneiss (Fig. 3a, c). Macroscopic evidence of partial melting is locally present in the mafic enclaves (Fig. 3b, d).

3 Previous descriptions of HP rocks in cDML

Indications of HP metamorphism of Maud Belt rocks have been described from H.U. Sverdrupfjella in western DML by Pauly et al. (2016). They estimated peak conditions of ca. 930 °C and 1.45 GPa based on thermobarometry recorded by high-Zr rutile and Ti in zircon. Timing of the HP metamorphism was estimated at 570 ± 7 Ma (U–Pb zircon age; Pauly et al., 2016). The presence of an HP event in H.U. Sverdrupfjella has also been suggested by Groenewald et al. (1995), Grantham et al. (1995) and Board et al. (2005) based on the occurrence of garnet + clinopyroxene + quartz + plagioclase + rutile in mafic rocks. The presence of clinopyroxene with plagioclase exsolution lamellae was interpreted to represent former omphacite, and a minimum pressure of 1.3–1.4 GPa was estimated based on the reintegrated omphacite composition (Board et al., 2005).

Possible relicts of an early HP assemblage have been reported from Gjelsvikfjella (Fig. 2a) by Bisnath and Frimmel (2005). Here, garnet amphibolite contains amphibole + plagioclase symplectite, which was interpreted to have formed after former clinopyroxene. A garnet amphibolite from Filchnerfjella (Fig. 2a) contains relicts of the early assemblage amphibole (ferrotschermakite) + garnet + kyanite (Engvik and Elvevold, 2004; Elvevold and Engvik, 2013), which is indicative of HP, possibly eclogite-facies, metamorphism. Reliable estimates for peak pressure were not made for the garnet amphibolites from Gjelsvikfjella or from Filchnerfjella.

Palmeri et al. (2018) describe HP granulite-facies metamorphism preserved in ultramafic rocks from Conradfjella. P–T modeling yielded 960–970 °C and ca. 1.5–1.7 GPa for the peak conditions, which were followed by decompression to ca. 0.4 GPa and 750–850 °C. The clockwise P–T path was ascribed to the Pan-African orogeny.

In summary, scattered evidence of an early HP metamorphic stage is preserved in mafic and ultramafic rocks of the Maud Belt from H.U. Sverdrupfjella in the west to Conradfjella in the east (see also Godard and Palmeri, 2013). At some localities, mineral textures indicative of former eclogite-facies metamorphism have been recognized; however, true eclogites with garnet + omphacite-bearing assemblages have not been documented yet. The age of the early HP metamorphism in DML is still only loosely constrained to ca. 570 Ma.

4 Analytical methods

Samples for the present study were collected during a research expedition by the Norwegian Polar Institute in 2018. The locality for the analyzed samples is marked in Fig. 2b. The investigated samples are stored in the rock repository of the Norwegian Polar Institute (NPI) in Tromsø, Norway, and identified by five-digit numbers that are catalogued in an NPI database. Mineral abbreviations in the text and the figures follow Whitney and Evans (2010).

4.1 Geochemistry

Mineral chemistry was analyzed using a Cameca SX100 electron microprobe with five wavelength-dispersive spectrometers at the Department of Geosciences, University of Oslo, Norway. The analyses were performed under conditions of 15 kV accelerating voltage, a 15 nA sample current and a focused beam. Standardization was made on a selection of synthetic and natural minerals and oxides. Matrix corrections were calculated using the PAP procedure (Pouchou and Pichoir, 1984). Representative mineral compositions are given in the Supplement, Tables S1–S6.

Compositional element-distribution maps (X-ray maps) were acquired in order to study zoning characteristics. The

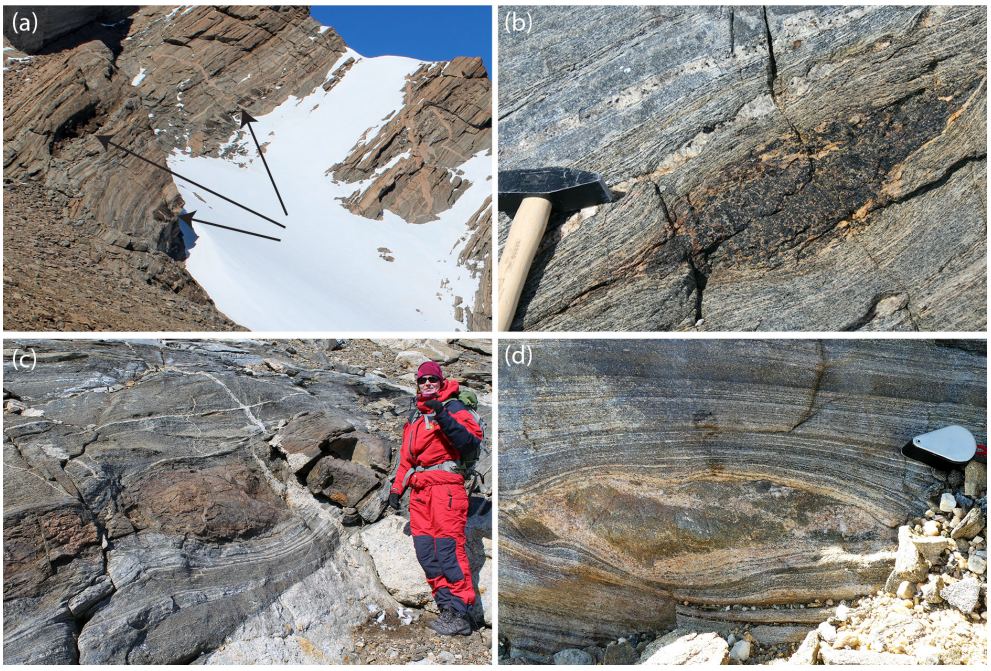

Figure 3. Field relations, Jutuldalen. **(a)** Strongly deformed orthogneiss with lenses and pods of mafic rocks (at arrows). The orthogneiss and mafic lenses are intruded by abundant post-tectonic granitic dikes. **(b)** Small enclave of garnet amphibolite. **(c)** Sample locality of the mafic enclaves NP03016A, NP03016B, NP03016C, NP03971 and NP03972. **(d)** Mafic enclave with melt texture.

X-ray maps were obtained using five wavelength-dispersive X-ray spectroscopy (WDS) spectrometers by moving the sample under a stationary beam and collecting X-ray counts in a grid pattern. Analytical operation conditions for the X-ray maps were an accelerating voltage of 15 kV, a beam current of 40 nA and counting time of 50 ms.

Whole rock compositions (major and trace elements) were analyzed at the Geological Survey of Norway (Supplement, Table S7). Major elements were measured on tablets and fused glass beads prepared by 1 : 7 dilution with lithium tetraborate. The samples were analyzed on a PANalytical Axios X-ray fluorescence (XRF) spectrometer equipped with a 4 kW Rh X-ray end-window tube, using common international standards for calibration. Trace element analyses (Supplement, Table S8) were performed using a Thermo Scientific Element XR single-collector, high-resolution ICP-MS instrument linked to a New Wave UP193-FX 193 nm excimer laser ablation system.

4.2 U–Pb geochronology

U–Pb analysis of zircon was performed in situ on two thin sections. SEM-backscattered and cathodoluminescence imaging was carried out to reveal the internal structure of the zircons prior to dating. Analysis spots were carefully chosen after considering detailed transmitted, reflected and cathodoluminescence imaging, in order to avoid inclusions and cracks. The U–Pb data are given in the Supplement, Table S9.

The U–Pb zircon analyses were carried out on a high-resolution, single-collector (HR-SC) ICP-MS instrument (Nu Instruments Attom ES) attached to a 193 nm ArF excimer laser ablation system (RESOlution M-50 LR) at the Bergen Geoanalytical Facility, University of Bergen, Norway. The analytical details of the system and data reduction methods are documented in the Supplement, Table S10. Prior to the analytical session, the operating conditions of the LA-ICP-MS instrument were calibrated doing raster ablation on the standard reference materials NIST612 or 91500, optimizing the instrument settings to achieve maximum signal counts and stability while simultaneously minimizing the production of oxide species $((^{254}\mathrm{UO} / {}^{238}\mathrm{U}) \times 100) < 0.1$. The zircon grains underwent laser ablation for a duration of 30 s, preceded by 15 s of blank measurement. A spot size of 19 µm, a repetition rate of 5 Hz and a fluence of 3 J cm^{-2} were employed during the ablation process. Time-resolved peak-jumping mode was utilized to collect data for specific masses, including $^{202}\mathrm{Hg} + {}^{204}(\mathrm{Pb} + \mathrm{Hg})$, $^{206}\mathrm{Pb}$, $^{207}\mathrm{Pb}$, $^{208}\mathrm{Pb}$, $^{232}\mathrm{Th}$, $^{235}\mathrm{U}$ and $^{238}\mathrm{U}$. To address the non-linear transition between the two counting modes in the detector, a conversion method was applied for measuring $^{238}\mathrm{U}$ when it surpassed 2×106 counts, triggering the attenuated mode. In this case, the $^{238}\mathrm{U}$ counts were calculated from the $^{235}\mathrm{U}$ counts by multiplying them by a constant factor of 137.818, as established by Hiess et al. (2012). This recalculation step occurred after data collection but before data reduction,

using a customized Python script. Data reduction was carried out using Iolite 4 (version 4.8.1) in accordance with the U–Pb geochronology data reduction scheme developed by Paton et al. (2010, 2011). The data reduction methodology followed the procedures outlined by Paton et al. (2011) and included several correction steps. Corrections were applied for gas blank, laser-induced elemental fractionation of Pb and U and instrument mass bias. To correct both blank counts and instrumental bias, an automatic spline function was employed. For the correction of down-hole element fractionation, a smoothed cubic line function was used. No common Pb correction was applied to the data; it was only monitored. The remaining element fractionation and instrumental mass bias were corrected by normalizing to the natural zircon reference material 91500 (Wiedenbeck et al., 1995). For quality control, regular measurements of the zircon reference materials GJ1 (Jackson et al., 2004) and Plešovice (Sláma et al., 2008) were conducted, and their values are reported in the Supplement, Table S10. The primary reference zircon 91500 and other secondary reference zircons were analyzed after every six to eight ablation spots. For the generation of Wetherill plots, the IsoplotR program (Vermeesch, 2018) was utilized.

Three age standards were regularly measured during the analytical session. The two secondary reference materials were reproduced within 2 % of their reported thermal ionization mass spectrometry (TIMS) age. Age uncertainties in the text are 2σ.

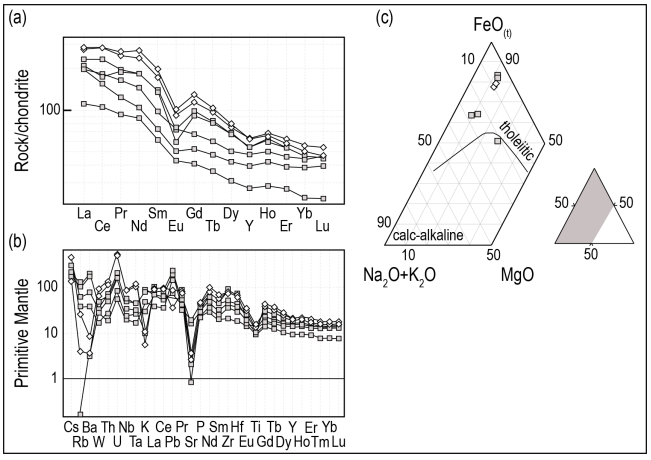

Figure 4. Plots of whole rock major and trace element compositions. Diamonds denote samples NP03971A and NP03971B; grey squares denote other mafic lithologies from Jutulsessen. **(a)** Spider diagram showing rare-earth element (REE) concentrations normalized to chondrite (McDonough and Sun, 1995). **(b)** Spider diagram showing high-field-strength element (HFSE) and REE contents normalized to primitive mantle compositions (Sun and McDonough, 1989). **(c)** Ternary alkalis–FeO–MgO (AFM) diagram showing the compositional placement of samples NP03971A and NP03971B relative to mafic lithologies. The boundary line between tholeiitic and calc-alkaline series is after Rickwood (1989). The part of the diagram containing data is shown (grey-shaded area).

5 Results

5.1 Petrography

The following descriptions focus on the least retrogressed samples of HP mafic rocks enveloped in amphibolite-facies felsic gneiss from Jutuldalen. In addition, descriptions of the retrogressed amphibole-rich margin of the mafic rocks are included.

5.1.1 Major and trace element characteristics

The anhydrous core of a mafic enclave (sample NP03971A and NP03971B) is characterized by high total FeO (17.9 wt %–19.7 wt %), TiO_2 (3.0 wt %–3.3 wt %), P_2O_5 (0.9 wt %–1.0 wt %) and Zr (917–975 µg g^{-1}). The Fe–Ti-rich bulk chemistry is reflected in the high modal amount of ilmenite, as well as remarkably Fe-rich garnet, clinopyroxene and amphibole. Figure 4 shows analyses of the mafic enclave plotted together with other mafic lithologies from Jutulsessen. The mafic rocks show a moderate Eu anomaly (Fig. 4a) and a general enrichment in high-field strength elements and rare-earth elements relative to basaltic compositions (Fig. 4b). In the ternary alkalis–FeO–MgO (AFM) diagram, the samples of the mafic pod and the mafic lithologies plot in the tholeiitic field (Fig. 4c). This agrees with the interpretation that the protoliths are mostly juvenile arc-related magmas (e.g., Wang et al., 2020b).

5.1.2 Anhydrous core of mafic pod

The anhydrous core of the mafic pods is composed of garnet and dark ilmenite-rich blobs set in a finer-grained matrix of quartz, clinopyroxene and plagioclase with minor orthopyroxene, amphibole, apatite and zircon (Fig. 5a). A characteristic feature of the microtexture is the abundant fine-grained, vermicular symplectitic intergrowth of ilmenite + clinopyroxene ± orthopyroxene (Fig. 5b, c). The intergrowths comprise elongate lamellae of ilmenite set in clino- and/or orthopyroxene and are commonly mantled by a 10–50 µm wide rim of clino- or orthopyroxene, which is in optical continuity with that of the intergrowth. The symplectites are commonly surrounded by matrix quartz or plagioclase + clinopyroxene intergrowths and are not observed in direct contact with garnet. The unusual ilmenite-bearing intergrowths typically display an outline that suggests pseudomorphic replacement of a wedge-shaped precursor (Fig. 5a, b, c).

Another distinctive reaction texture is plagioclase + clinopyroxene intergrowths. Plagioclase is the host mineral and contains inclusions of clinopyroxene and, more rarely, orthopyroxene or amphibole (most probably as replacement products after clinopyroxene). The

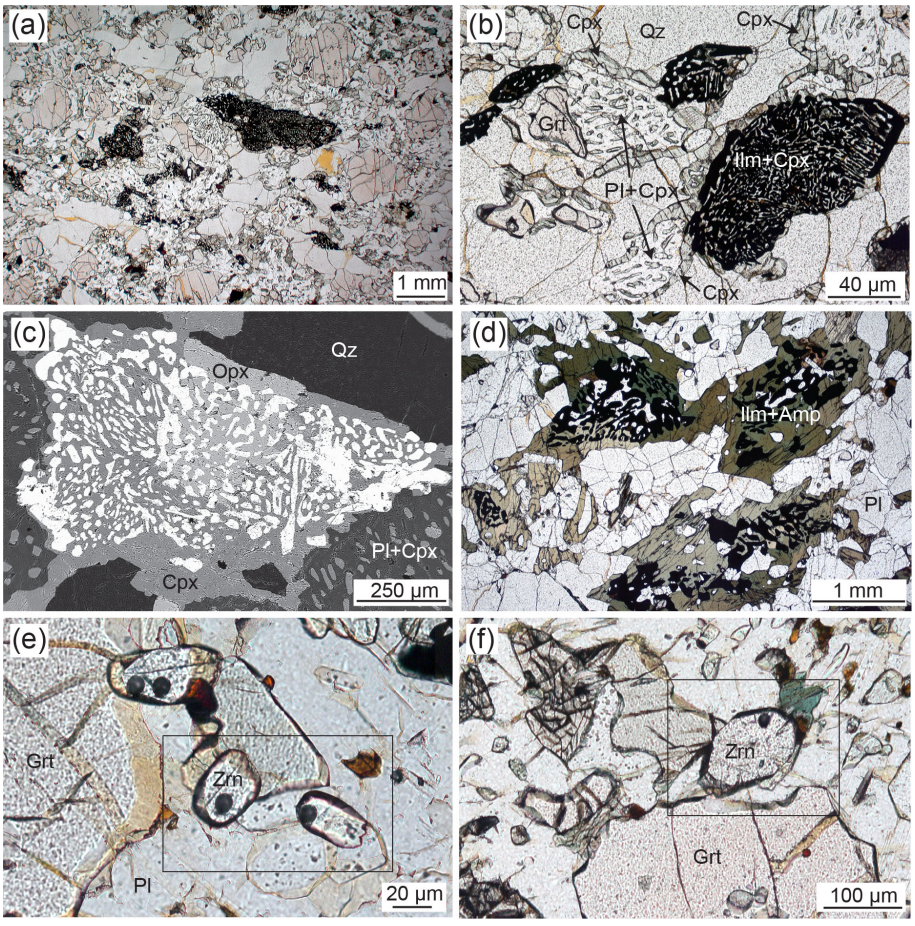

Figure 5. Thin-section microphotos (plane-polarized light) and backscattered electron (BSE) image of mafic enclaves. **(a)** Sample NP03016B from the anhydrous core of the mafic enclave comprises garnet (pink), ilmenite–pyroxene symplectites (black spots), quartz and minor plagioclase, clinopyroxene, and amphibole. Note the wedge-shaped ilmenite–pyroxene symplectite in the middle of the image. **(b)** Ilmenite–pyroxene symplectite and plagioclase–clinopyroxene intergrowth set in a quartz-rich matrix. The plagioclase–pyroxene intergrowth is mantled by a corona of clinopyroxene. Sample NP03016B. **(c)** BSE image of ilmenite–clinopyroxene symplectite and plagioclase–clinopyroxene intergrowth in a quartz matrix. Note that clinopyroxene has been replaced by orthopyroxene in the upper middle part of the symplectite. Sample NP03016A. **(d)** Ilmenite–pyroxene symplectites are surrounded and replaced by amphibole. The sample, NP03016C, is from the amphibolitized margin of the mafic enclave. **(e, f)** Microphotos of matrix zircons from sample NP03016A and NP03016B respectively that are dated with the LA-ICP-MS method; see also Fig. 8.

clinopyroxene inclusions appear as globules (10–20 µm) and worm-like lamellae resulting in a globular microtexture (Fig. 5b, c). The plagioclase + clinopyroxene symplectite is commonly mantled by a rim of clinopyroxene that seems to be in optical continuity with the clinopyroxene inclusions.

Garnet porphyroblasts comprise ca. 40 % of the sample volume. The mineral is anhedral, is 1–3 mm across, contains pervasive fractures transecting entire grains and has rounded to strongly embayed grain boundaries. Quartz, plagioclase, calcite, ilmenite, apatite, zircon, amphibole and rare clinopyroxene are present as unevenly distributed inclusions. Large garnets are commonly replaced and rimmed by a kelyphite of plagioclase or a discontinuous corona of plagioclase ± clinopyroxene ± orthopyroxene (Fig. 5a), whereas smaller garnet grains are associated with plagioclase + clinopyroxene intergrowths (Fig. 5b).

Except for rare inclusions in garnet, plagioclase is secondary in origin. Secondary plagioclase formed by replacement reactions in different textural settings: (i) in globular symplectite together with clinopyroxene and (ii) in kelyphite associated with clino- and orthopyroxene. Minor orthopyroxene is present as secondary grains replacing clinopyroxene in (i) the ilmenite-bearing symplectite and (ii) plagioclase-bearing intergrowths. Orthopyroxene is also present in the kelyphite replacing garnet. Retrograde amphibole replaces garnet and clino- and orthopyroxene. There is no evidence for the presence of primary orthopyroxene and amphibole. Apatite and zircon are present as accessory phases in the matrix (Fig. 5e, f).

5.1.3 Amphibolitized margins of mafic pods

Retrograde equilibration to amphibolite-facies assemblages is found along the margins of the mafic enclaves, adjacent to felsic veins and fractures where fluid influx has occurred (Fig. 3b). The amphibolitized margins are characterized by a granoblastic to nematoblastic texture. The grain size gradually increases from the inner anhydrous part of the enclaves to the outer retrogressed margin. The mineralogy of the margin is dominated by green amphibole, biotite, ilmenite, garnet and plagioclase. Former clinopyroxene and orthopyroxene are completely replaced by amphibole and biotite, and garnet is for the most part replaced by plagioclase and biotite. Ilmenite that was intergrown with pyroxene is present as inclusions within amphibole and is coarser grained than in the core region of the enclave (Fig. 5d). Grunerite is present as a late amphibole phase.

5.2 Mineral chemistry

5.2.1 Anhydrous core of mafic pods

Representative microprobe analyses of garnet, clino- and orthopyroxene, ilmenite, amphibole, and plagioclase are given in the Supplement, Tables S1–S6, and the mineral chemistry of pyroxene and amphibole is plotted in Fig. 6.

Garnet is almandine-rich with minor pyrope and spessartine. The mineral is characterized by a broad homogeneous interior with compositional zonation present along the crystal edges. Figure 7 displays element-distribution maps of a resorbed garnet that is surrounded by an inner corona of plagioclase and an outer corona of orthopyroxene and minor amphibole. The zoning is characterized by a rimward decrease in pyrope and grossular and increase in almandine, as well as a slight increase in spessartine. The core region is $Alm_{60-61}Grs_{25-26}Prp_{13-14}Sps_{01}$, whereas the rim composition is $Alm_{66-69}Grs_{22-24}Prp_{07-08}Sps_{03}$. The Fe / (Fe + Mg) ratio increases from 0.81 in the core to 0.91 at the rim. The broad homogenous core composition is related to intracrystalline diffusion at high temperatures, whereas the zoning along the rims is the result of diffusion related to garnet consumption. Clinopyroxene is present in several textural settings: (i) as rare inclusions in garnet porphyroblasts, (ii) intergrown with ilmenite, (iii) as globules and lamellae in plagioclase, (iv) in kelyphite surrounding garnet, and (v) as matrix grains. The composition of clinopyroxene is surprisingly uniform. Clinopyroxene included in garnet is diopside, whereas clinopyroxene in the other four textural positions is classified as magnesian hedenbergite. Some analyses of matrix clinopyroxene plot in the augite field (Fig. 6a). The jadeite component is negligible (< 2 mol % Jd). Ilmenite lamellae and globules in the symplectitic intergrowth with clino- and orthopyroxene are rich in Fe with very low MgO (0.12 wt %–0.18 wt %) and MnO (0.36 wt %–0.42 wt %). The Fe/Ti ratio ranges from 0.964 to 0.997. Orthopyroxene, which is present as a minor phase replacing clinopyroxene in the ilmenite–clinopyroxene symplectite and together with plagioclase in the kelyphite replacing garnet, is ferrosilite with X_{Mg} around 0.30. The Ti content of orthopyroxene is higher in the ilmenite-bearing symplectite than in the kelyphite (Table S3). Secondary plagioclase is present in two textural settings: (i) in kelyphite replacing garnet and (ii) intergrown with clinopyroxene. Plagioclase is strongly zoned in both textural positions, and the composition ranges from labradorite to bytownite (An_{53} to An_{82}). Plagioclase in the reaction rim surrounding garnet in Fig. 7 ranges from An_{48}–An_{67}. Rare inclusions of plagioclase in garnet are An_{60}. The calcic amphibole is ferro-ferri-hornblende and ferro-hornblende (Fig. 6c). Analyses of amphibole in garnet are tschermakite and magnesio-hornblende. Late amphibole, which occurs in the matrix as small grains on orthopyroxene, is ferro-hornblende and grunerite.

5.2.2 Amphibolitized margins of mafic pods

The green calcic amphibole that dominates the matrix is ferro-pargasite. The green amphibole is overgrown by a later, colorless grunerite with quartz exsolution lamellae. Analyzed plagioclase in kelyphite and the matrix is An_{40-43}. Matrix plagioclase is weakly zoned with a rimward decrease in the anorthite content. Biotite, which is formed by retrograde breakdown reactions, is Fe- and Ti-rich. The Fe / (Fe + Mg) values of matrix biotite range from 0.60 to 0.70, and Ti values are 0.47–0.60 atoms per formula unit.

5.3 Zircon U–Pb geochronology

Zircons are present throughout the matrix in the two investigated samples from the anhydrous mafic pod (NP03016A and NP03016B, sampled 0.5 m apart) (Fig. 5e, f). Three types of zircons are recognized based on CL characteristics: (i) as euhedral to subhedral prismatic grains with mostly oscillatory igneous growth zoning, reaching 300 µm in length; (ii) as small, rounded grains (< 60 µm) with irregular or complex zoning; and (iii) as subhedral to anhedral grains with metamorphic overgrowths. The three types of zircons are present in both thin sections (Table S9); however, most zircon grains are prismatic with oscillatory growth zoning (type i). Only a few small, rounded zircons (type ii) were recognized. The Th/U ratios of the three different zircon types are mainly undifferentiable, ranging from 0.3 to 0.8. Only one analysis from a discordant type (ii) zircon has a significantly lower value of 0.02.

5.3.1 Anhydrous garnet–clinopyroxene rock (NP03016A)

Twenty analyses were conducted on matrix zircons in sample NP03016A. Two analyses were excluded because of high discordance. The two youngest ages are concordant and

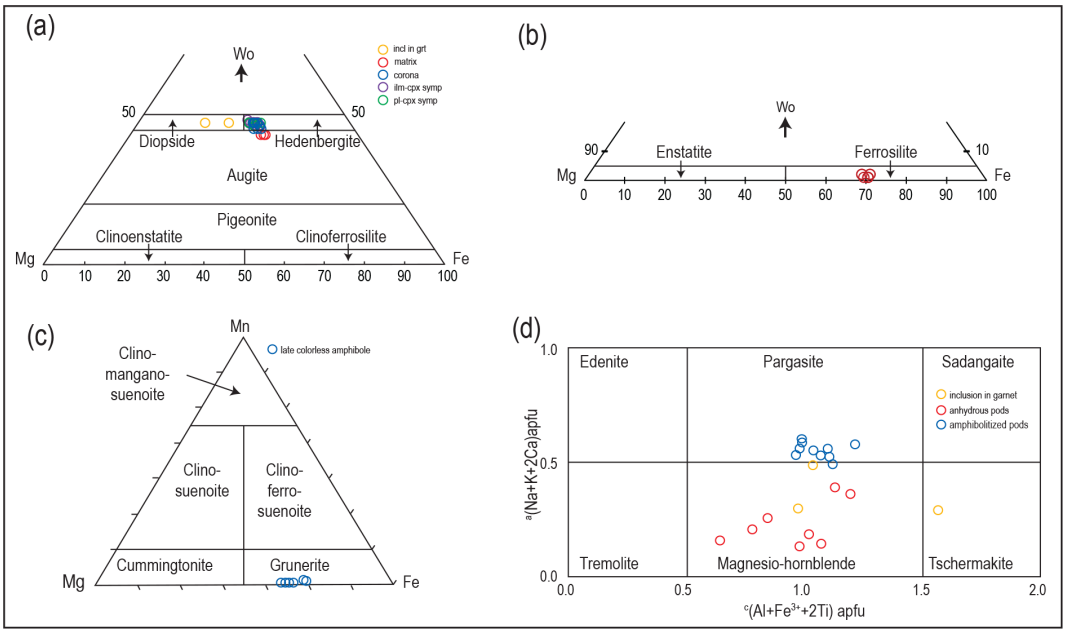

Figure 6. **(a)** Clinopyroxene and **(b)** orthopyroxene classification in the Wo–Fs–En diagrams, **(c)** Mg–Fe–Mn amphibole classification, and **(d)** Ca-amphibole classification after Hawthorne et al. (2012).

were obtained from small, rounded, complexly zoned zircons (Figs. 8a, 5e). The concordia age of the two youngest ages is 568 ± 4 Ma. Elongated and prismatic, oscillatory- and sector-zoned zircons yield discordant ages that range from the late Mesoproterozoic to early Neoproterozoic. When forcing a discordia line through 568 ± 4 Ma, the upper intercept is $1115 + 23/-39$ Ma (mean square weighted deviation (MSWD) = 2.9). The observed scatter in the older ages is probably a combination of multiple ancient and recent lead loss events.

5.3.2 Anhydrous garnet–clinopyroxene rock (NP03016B)

Twenty-two analyses were carried out on matrix zircons in sample NP03016B. Four analyses were highly discordant and are not further considered. Most analyses are older and of late Mesoproterozoic to early Neoproterozoic age. These ages were recorded from elongated and prismatic, oscillatory- and sector-zoned zircons. A young age population of four zircons was recorded from zircon rims and a rounded complexly zoned grain. The two most concordant analyses of these were obtained from a CL-bright overgrowth (Figs. 8b, 5f) and provide a concordia age of 514 ± 4 Ma. The remaining analyses define a discordia line with an upper intercept at ca. 1117 Ma when forced through 514 ± 4 Ma.

6 Discussion

6.1 Petrological interpretation

The presence of symplectite and kelyphite clearly indicates a lack of textural equilibrium. The wide-ranging composition of plagioclase suggests that equilibrium is at best only domainal. Symplectites are delicate textures that are easily destroyed by deformation and are, therefore, generally preserved in low-strain areas such as the protected cores of the mafic lenses. The preservation of symplectite also suggests limited availability of metamorphic fluid. In the presence of an interconnected fluid phase, mass transport can take place by grain boundary diffusion much faster than by solid state diffusion. Restricted diffusion will thus result in local equilibrium, which is typical of symplectite reactions. The small modal amount of retrograde amphibole in the core samples also supports restricted fluid infiltration during retrogression.

6.1.1 Precursor of ilmenite + clinopyroxene symplectite

The least retrogressed samples are characterized by abundant and conspicuous symplectite of ilmenite + clinopyroxene. The reactant phase is not preserved within the symplectite. Symplectitic intergrowth of ilmenite + clinopyroxene is not commonly reported; however, titanite replaced by ilmenite + clinopyroxene has been described from retrogressed eclogites and HP granulites elsewhere (Carswell et al., 1996; O'Brien and Rötzler, 2003; Faryad et al., 2006; Marsh and Kelly, 2017).

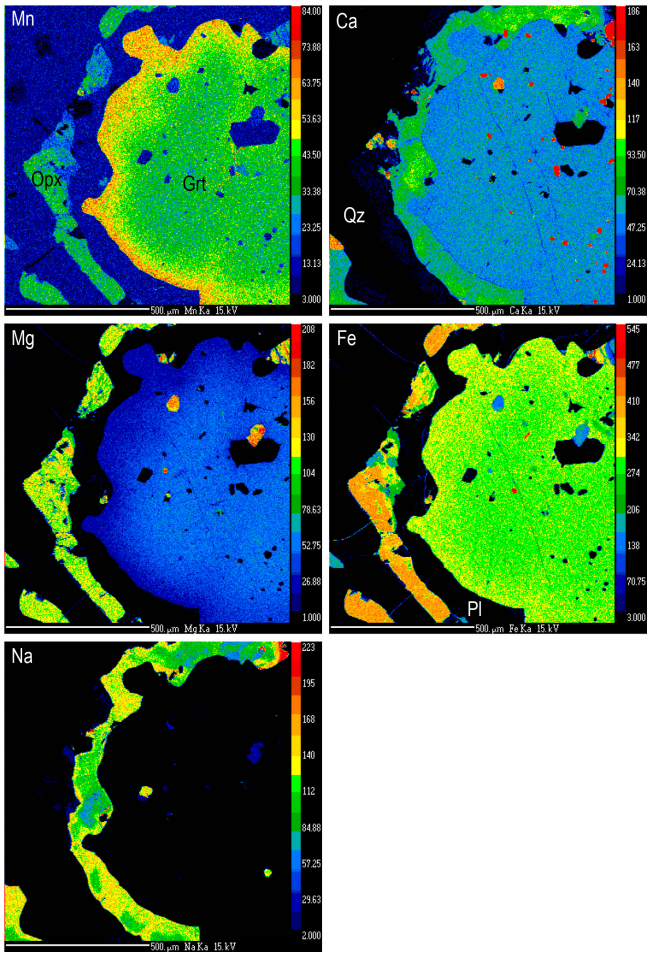

Figure 7. Element-distribution maps in garnet and surrounding reaction rim consisting of plagioclase and pyroxene, sample NP03971. Red colors show areas of high concentration, while blue colors represent areas of low concentration (black is very low concentrations). Garnet is relatively homogenous in the core region. The zoning is characterized by a slight rimward increase in Mn and Fe and a decrease in Mg. The Na map shows that the plagioclase rim surrounding garnet is strongly zoned. The high-Na area (red) is An_{48}, whereas the low-Na area (blue) is An_{67}.

Faryad et al. (2006) described the presence of ilmenite + clinopyroxene symplectite in retrogressed eclogite from the Moldanubian Zone in the Czech Republic. The ilmenite + clinopyroxene symplectite replaces titanite that is in contact with omphacite and garnet. These authors interpret the symplectite as forming during decompression and heating of eclogite under granulite-facies conditions. The intergrowths are further assumed to have formed by allochemical reactions between titanite and adjacent garnets. Anatectic HP mafic granulites from the Grenville Province, Ontario, contain large titanite grains mantled by fine-grained ilmenite + clinopyroxene symplectite (Marsh and Kelly, 2017). Formation of the symplectite is related to decompression at high temperature (ca. 750 °C). Similar textures have also been described from HP granulite from Granulitgebirge in Germany (O'Brien and Rötzler, 2003), while Carswell et al. (1996) reported symplectite of ilmenite + amphibole after Al-rich titanite, the latter coexisting with omphacite, garnet and coesite from the Dabieshan, China.

Based on the reports described above, we interpret the ilmenite + clinopyroxene symplectite to have formed from titanite. The wedge-shaped outline of the intergrowth, which resembles titanite, supports this interpretation. The symplectite is most probably the result of an allochemical reaction between titanite and surrounding matrix minerals, involving compositional change on the scale of the symplectitic replacement.

Al-rich titanite is reported from a variety of eclogites and associated HP rocks (e.g., Smith, 1980; Franz and Spear, 1985; Krogh et al., 1990; Hirajima et al., 1992; Carswell et al., 1996; Elvevold et al., 2014). Likewise, experimental data have shown that aluminous titanite can be produced at elevated pressure (Troitzsch and Ellis, 1999, 2002). Al-rich titanite may also form in the amphibolite facies during prograde metamorphism by reactions that involve ilmenite, quartz and clinopyroxene or amphibole (Harlov et al., 2006).

6.1.2 Precursor to the globular plagioclase + clinopyroxene symplectite

Globular plagioclase + clinopyroxene symplectite is widespread in the matrix. The anorthite-rich plagioclase (An_{53}–An_{79}) in the intergrowth does not support formation after former omphacite. The intergrowths are formed in the vicinity of garnet and the ilmenite-bearing symplectite and may have been formed by a complex reaction between garnet + titanite + quartz to form ilmenite + clinopyroxene symplectite (titanite) and plagioclase + clinopyroxene symplectites (after garnet).

6.2 *P–T–t* evolution

6.2.1 Metamorphic evolution

The *P–T–t* evolution of the mafic pods is given in Fig. 9. The peak-pressure assemblage in the investigated samples is interpreted to consist of garnet, titanite, clinopyroxene and quartz. Plagioclase was most likely not part of the peak-pressure assemblage, which suggests that the peak pressures were above that of the plagioclase stability field. We suggest that the investigated rocks entered the *P–T* field of HP granulite facies. The HP stage corresponds to the eclogite-facies to HP granulite-facies metamorphism as defined by Brown (2007, 2009). Eclogite-facies to HP granulite-facies metamorphism is characterized by medium-temperature eclogite-facies or HP granulite-facies mineral assemblages, where peak temperature generally is achieved *after* maximum pressure.

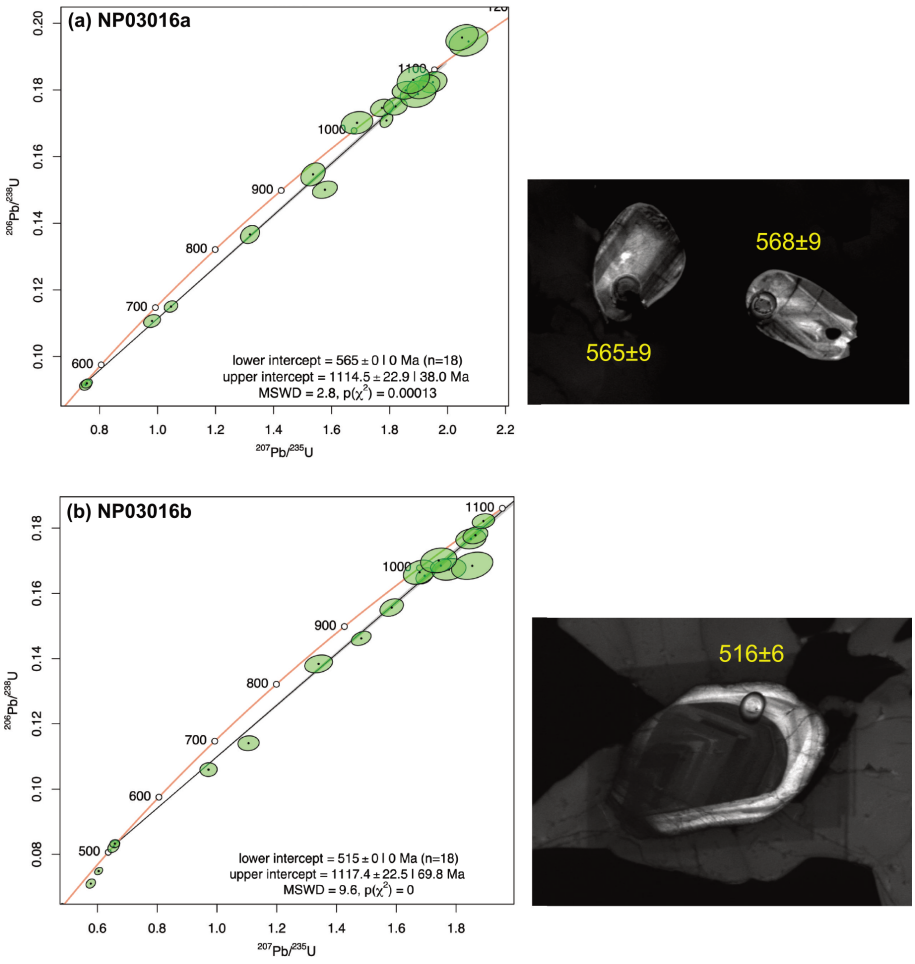

Figure 8. U–Pb zircon in situ analyses of two samples with examples of the three zircon types occurring. **(a)** Eighteen of a total of 20 analyses of sample NP03016A. The analyses straddle a poorly defined discordia line. The two youngest concordant analyses from small, rounded zircons provide a concordia age of 568 ± 4 Ma. The remaining analyses are roughly aligned along a discordia line that when forced through 568 ± 4 Ma, has an intercept at ca. 1115 Ma. **(b)** Eighteen of 22 analyses of sample NP03016B. Four analyses were excluded because of high discordance and/or high common Pb. Most analyses provide late Mesoproterozoic ages, and some straddle a discordia line. The four youngest analyses are from zircon rims (type-3 zircon) that surround an oscillatory-zoned core (type-1 zircons). Two concordant analyses of the young age group provide a concordia age of 514 ± 4 Ma. The majority of analyses straddle a discordia line that, when forced through 514 ± 4 Ma, has an upper intercept at ca. 1118 Ma. The latter age most likely indicates the crystallization age of the protolith, whilst the age of ca. 514 Ma is interpreted as best representing the age of metamorphism zircon overgrowth–recrystallization.

The peak-pressure phases are replaced by lower-pressure assemblages. The ilmenite + clinopyroxene symplectite and the kelyphite replacing garnet indicate that decompression took place at elevated temperatures. Previous studies have shown that the metamorphic evolution of the high-grade rocks of the Maud Belt in central Dronning Maud Land is characterized by a clockwise *P*–*T* evolution with a steep decompression segment (Board et al., 2005; Bisnath and Frimmel, 2005; Elvevold and Engvik, 2013; Pauly et al., 2016; Palmeri et al., 2018; Elvevold et al., 2020). It is, however, essential to recognize that deduced *P*–*T* paths may give the impression of an isothermal decompression rather than heating during decompression if the early lower temperature of the HP facies is no longer recoverable. The *P*–*T* path of the mafic pods studied herein may possibly have moved towards higher temperature during decompression from peak pressure.

High-grade and anatectic rocks are present along the length of the Maud Belt. The obvious textural and compositional disequilibrium in the rocks studied here makes use of conventional geothermobarometry and pseudosection modeling difficult. However, calculated phase equilibria in granulites from elsewhere in the Maud Belt have recorded peak temperatures in the range of 800–950 °C (Elvevold and Engvik, 2013; Pauly et al., 2016; Palmeri et al., 2018; Elvevold et al., 2020), which resulted in widespread anatexis of pelitic and quartzo-feldspathic gneisses.

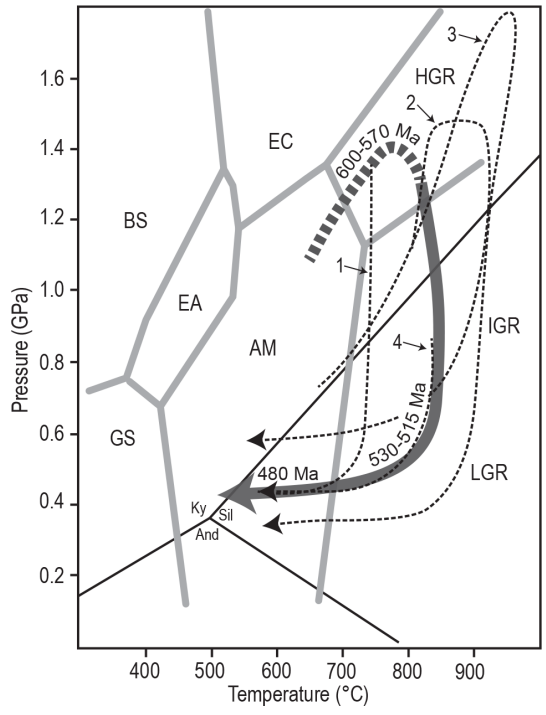

Figure 9. The diagram shows the suggested P–T–t path for the mafic enclaves from Jutuldalen (thick arrow). The dashed arrows that are published P–T paths from other areas within the Maud Belt in cDML are shown for comparison: (1) Board et al. (2005), (2) Pauly et al. (2016), (3) Palmeri et al. (2018) and (4) Elvevold et al. (2020). The onset of Pan-African metamorphism is constrained at 600–570 Ma (this study; Jacobs et al., 1998, 2003b; Pauly et al., 2016; Baba et al., 2015), followed by a younger zircon growth event at 530–515 Ma (this study; Jacobs et al., 1998, 2003b; Baba et al., 2015). The cooling through 550–650 °C dated to 480 Ma is $^{40}Ar/^{39}Ar$ hornblende age (Hendriks et al., 2013). The facies grid is after Oh and Liou (1998). Abbreviations: GS: greenschist facies, BS: blueschist facies, EA: epidote amphibolite facies, AM: amphibolite facies, EC: eclogite facies, HGR: high-pressure granulite facies, IGR: intermediate-pressure granulite facies, LGR: low-pressure granulite facies.

The host orthogneisses to the mafic enclaves, as well as the margins of the enclaves, are characterized by amphibolite-facies assemblages. The late stages of the P–T evolution of the Maud Belt involved a final, near-isobaric-cooling segment, which has been proposed by Elvevold et al. (2020) for supracrustal gneisses from Mühlig-Hofmannfjella and by Pauly et al. (2016) for granulites from H.U. Sverdrupfjella.

6.2.2 Zircon U–Pb data

Three age populations of zircon were identified in the HP granulites: 1150–1000 Ma, ca. 568 and ca. 514 Ma. Most analyses record Mesoproterozoic ages, which most likely indicate the igneous crystallization age of the magmatic protolith. These ages are in agreement with the existing literature of the late Mesoproterozoic magmatic event in Gjelsvikfjella (Paulsson and Austrheim, 2003; Bisnath et al., 2006) and other areas within the Maud Belt (e.g., Jacobs et al., 1998, 2003a, b; Wang et al., 2020b). The upper-intercept age of ca. 1117 Ma is very similar to Umkondo large igneous province (LIP) ages of the Kalahari plate (e.g., Hanson et al., 2004). The protolith of the studied mafic boudins may represent dikes related to this LIP.

The Pan-African ages of ca. 568 and ca. 514 Ma most probably relate to late Neoproterozoic tectono-metamorphic reworking. Although the dataset recorded herein is relatively small, the new LA-ICP-MS zircon ages agree well with available published data. Jacobs et al. (1998) reported two metamorphic U–Pb zircon age groups at ca. 570–550 and ca. 530–515 Ma from various lithologies from Orvinfjella and Wohlthatmassivet. Two sets of Pan-African zircon ages, 598–599 and 522–525 Ma, have also been recorded from Hochlinfjellet and Filchnerfjella (Baba et al., 2015). Other ages of 565–570 Ma have been reported from H.U. Sverdrupfjella (Board et al., 2005; Pauly et al., 2016), Hochlinfjellet (Elvevold et al., 2020) and Humboldtfjella (Mikhalsky et al., 1997).

It is tempting to relate the ca. 568 Ma age to the HP stage; however, U–Pb ages from HP rocks cannot a priori be assumed to date the timing of the HP metamorphism (e.g., Kohn et al., 2015). Mineral reactions over a range of metamorphic grades play an important role in the dissolution and growth of metamorphic zircon. Zircon growth in metamorphic mafic rocks is commonly associated with Fe–Ti oxide transition due to the similar chemical properties of Zr and Ti (e.g., Bingen et al., 2001; Austrheim et al., 2008). With no further data available, we can only speculate that the small, ca. 565 Ma zircons may have formed by release of zirconium during decomposition of Ti-bearing silicates, such as titanite (as discussed above), and oxide. In such cases, the 568 Ma age would be related to the decompression stage rather than to the peak-pressure stage (Fig. 9).

The ca. 514 Ma age is comparable to the younger Pan-African age group (530–515 Ma; Jacobs et al., 1998, 2003b; Baba et al., 2015). Metamorphic zircon rims from a migmatitic granodioritic gneiss located at Jutulhogget (Fig. 1) yield a U–Pb zircon age of 504 ± 6 Ma that is interpreted as the time of migmatization (Paulsson and Austrheim, 2003). Crystallization of anatectic melt during cooling from peak temperature is expected to be the main mechanism for zircon growth in supra-solidus metamorphic rocks (e.g., Kohn et al., 2015; Yakymchuk et al., 2017). According to Kohn et al. (2015), most metamorphic zircons will grow during oxide transitions and anatectic melt crystallization. Their equilibrium Zr mass balance models for hydrous MORB indicate that zircon is largely produced during retrograde metamorphism. The metamorphic rims that record an age at ca. 514 Ma could thus relate to the crystallization of anatectic melts or, alternatively, to reactions involving the breakdown of zirconium-bearing phases such

as clinopyroxene, ilmenite or garnet (Fraser et al., 1997; Bea et al., 2006; Baldwin, 2015; Rubatto, 2017).

The range of ages within each of the two Pan-African age groups (600–550 and 530–505 Ma) may relate to different zircon-forming reactions. The Zr mass balance models by Kohn et al. (2015) predict that zircon growth can occur over a range of P–T conditions depending on the bulk composition and the P–T path. The older Pan-African age group within DML are taken to date the main period of crustal thickening during the East African–Antarctic Orogen. The clockwise P–T path, which is characteristic of the Pan-African evolution, is consistent with thermal models of the thickening of continental crust in collision zones (e.g., Thompson and Connolly, 1995). The younger Pan-African metamorphic ages (530–505 Ma) are synchronous with the large volumes of post-collisional, late Cambrian granitoid magmatism around 530–490 Ma that are evident throughout central DML (e.g., Jacobs et al., 2003; Wang et al., 2020a). The high-temperature metamorphism and following widespread magmatism have been related to post-collisional delamination and orogenic collapse (Jacobs et al., 2008).

7 Concluding remarks

The new data in this study largely confirm the geodynamic implication outlined by others for the region (e.g., Jacobs et al., 2020). The mafic rocks from Jutulsessen, Gjelsvikfjella, extends the presence of HP rocks in the Maud Belt. The physical conditions necessary for the development of the HP granulite-facies metamorphism of the Maud Belt were attained during continent–continent collision along the East African–Antarctic Orogen. The continental collision of the eastern margin of the Kalahari (the Maud Belt) and the TOAST started in the Ediacaran (600–570 Ma) and was followed by decompression and high-T–low-P metamorphism. The high-T metamorphism partly erased the peak-P assemblages because the rocks were not exhumed fast enough to overcome the effects of thermal relaxation. The amphibolite-facies metamorphism and the associated post-tectonic magmatism (530–490 Ma) are related to extensional tectonics with a collapsing orogen accompanied by upwelling of a hot asthenosphere through delamination of the orogenic root.

Data availability. The investigated samples are stored in the rock repository of the Norwegian Polar Institute (NPI) in Tromsø, Norway, and are identified by five-digit numbers that are catalogued in an NPI database. Raw data can be provided by the corresponding author upon request.

Supplement. The supplement related to this article is available online at: https://doi.org/10.5194/ejm-35-969-2023-supplement.

Author contributions. Fieldwork was performed by SE, JJ, AKE and PIM. SE, JJ and LERP performed measurements and analyzed the data; SE wrote the original manuscript with contributions from JJ, LERP and ØS; all co-authors reviewed and edited the manuscript.

Competing interests. The contact author has declared that none of the authors has any competing interests.

Disclaimer. Publisher's note: Copernicus Publications remains neutral with regard to jurisdictional claims made in the text, published maps, institutional affiliations, or any other geographical representation in this paper. While Copernicus Publications makes every effort to include appropriate place names, the final responsibility lies with the authors.

Special issue statement. This article is part of the special issue "(Ultra)high-pressure metamorphism, from crystal to orogenic scale". It is a result of the 14th International Eclogite Conference (IEC-14) held in Paris and Lyon, France, 10–13 July 2022.

Acknowledgements. The fieldwork for this study was carried out during the geological expedition 2017–2018 and organized by the Norwegian Polar Institute (NPI). We thank the Operation and Logistic Department at NPI and our field guide Sveinung Toppe for logistical support during the fieldwork. The work has benefit from additional support by the Geological Survey of Norway and the University of Bergen. We acknowledge Muriel Erambert for help with the electron microprobe analysis at the University of Oslo. Valuable and constructive reviews from Jane Gilotti, Antonio Langone and Gaston Godard helped us improve the paper.

Financial support. The geological expedition to Dronning Maud Land was financed by the Norwegian Polar Institute.

Review statement. This paper was edited by Gaston Godard and reviewed by Jane Gilotti and Antonio Langone.

References

Anderson, E. D. and Moecher, D. P.: Omphacite breakdown reactions and relation to eclogite exhumation rates, Contrib. Mineral. Petr., 154, 253–277, https://doi.org/10.1007/s00410-007-0192-x, 2007.

Austrheim, H., Putnis, C. V., Engvik, A. K., and Putnis, A.: Zircon coronas around Fe–Ti oxides: a physical reference frame for metamorphic and metasomatic reactions, Contrib. Mineral. Petr., 156, 517–527, https://doi.org/10.1007/s00410-008-0299-8, 2008.

Baba, S., Hokada, T., Kaiden, H., Dunkley, D. J., Owada, M., and Shiraishi, K.: SHRIMP zircon U-Pb dating of

sapphirine-bearing granulite and biotite hornblende gneiss in the Schirmacher Hills, east Antarctica: implications for Neoproterozoic ultrahigh-temperature metamorphism predating the assembly of Gondwana, J. Geol., 118, 621–39, 2010.

Baba, S., Horie, K., Hokada, T., Owada, M., Adachi, T., and Shiraishi, K.: Multiple collisions in the East African-Antarctic Orogen: Constraints from timing of metamorphism in the Filchnerfjella and Hochlinfjellet terranes in central Dronning Maud Land, J. Geol., 123, 55–78, 2015.

Baldwin, S. L.: Highlights and breakthroughs. Zircon dissolution and growth during metamorphism, Am. Mineral., 100, 1019–1020, https://doi.org/10.2138/am-2015-5279, 2015.

Bea, F., Montero, P., and Ortega, M.: A LA–ICP–MS evaluation of Zr reservoirs in common crustal rocks: Implications for Zr and Hf geochemistry, and zircon-forming processes, Can. Mineral., 44, 693–714, https://doi.org/10.2113/gscanmin.44.3.693, 2006.

Bingen, B., Austrheim, H., and Whitehouse, M.: Ilmenite as a source for zirconium during high-grade metamorphism? Textural evidence from the Caledonides of western Norway and implications for zircon geochronology, J. Petrol., 42, 355–375, 2001.

Bisnath, A. and Frimmel, H. E.: Metamorphic evolution of the Maud Belt: $P-T-t$ path for high-grade gneisses in Gjelsvikfjella Dronning Maud Land, East Antarctica, J. Afr. Earth Sci., 43, 505–524, 2005.

Bisnath, A., Frimmel, H. E., Armstrong, R. A., and Board, W. S.: Tectono-thermal evolution of the Maud Belt: new SHRIMP U-Pb zircon data from Gjelsvikfjella, Dronning Maud Land, East Antarctica, Precambrian Res., 150, 95–121, 2006.

Board, W. S., Frimmel, H. E., and Armstrong, R. A.: Pan-African tectonism in the Western Maud Belt: $P-T-t$ path for high-grade gneisses in the H.U. Sverdrupfjella, East Antarctica, J. Petrol., 46, 671–699, 2005.

Boland, J. and Van Roermund, H.: Mechanisms of exsolution in omphacites from high temperature, type b, eclogites, Phys. Chem. Miner, 9, 30–37, 1983.

Brown, M.: Metamorphism, plate tectonics, and the supercontinent cycle, Earth Sci. Front., 14, 1–18, 2007.

Brown, M.: Metamorphic patterns in orogenic systems and the geological record, in: Accretionary Orogens in Space and Time, edited by: Cawood, P. A. and Kröner, A., Geol. Soc. Lond. Spec. Publ., 318, 37–74, 2009.

Carswell, D. A. (Ed.): Eclogite facies rocks, Blackie, USA, ISBN 0-216-92687-4, 1990.

Carswell, D. A., Wilson R. N., and Zhai, M.: Ultra-high pressure aluminous titanites in carbonate-bearing eclogites at Shuanghe in Dabieshan, central China, Mineral. Mag., 60, 461–471, 1996.

Cox, R. and Indares, A.: Transformation of Fe–Ti gabbro to coronite, eclogite and amphibolite in the Baie du Nord segment, Manicouagan Imbricate Zone, eastern Grenville Province, J. Metamorph. Geol., 17, 537–555, https://doi.org/10.1046/j.1525-1314.1999.00216.x, 1999.

Elvevold, S. and Gilotti, J. A.: Pressure-temperature evolution of retrogressed kyanite eclogites, Weinschenk Island, North-East Greenland Caledonides, Lithos, 53, 127–147, 2000.

Elvevold, S. and Engvik A. K.: Pan-African decompressional P-T path recorded by granulites from central Dronning Maud Land, Antarctica, Miner. Petrol., 107, 651–664, 2013.

Elvevold, S., Engvik, A. K., Abu-Alam, T. S., Myhre, P. I., and Corfu, F.: Prolonged high-grade metamorphism of supracrustal gneisses from Mühlig-Hofmannfjella, central Dronning Maud Land (East Antarctica), Precambrian Res., 339, 105618, https://doi.org/10.1016/j.precamres.2020.105618, 2020.

Elvevold, S., Engvik, A. K., Hansen, C., Jacobs, J., Meiklejohn, I., Myhre, P. I., and Rudolph, E.: Geological map of Jutulsessen 1 : 50 000, Norsk Polarinstitutt Temakart Nr. 54, 385-401, 2021.

Elvevold, S., Ravna, E. J. K., Nasipuri, P., and Labrousse, L.: Calculated phase equilibria for phengite-bearing eclogites from NW Spitsbergen, Svalbard Caledonides, in: New Perspectives on the Caledonides of Scandinavia and Related Areas, edited by: Corfu, F., Gasser, D., and Chew, D. M., Geol. Soc. Lond. Spec. Publ., 390, 385–401, https://doi.org/10.1144/SP390.4, 2014.

Engvik, A. K. and Elvevold, S.: Pan-African extension and near-isothermal exhumation of a granulite facies terrain, Dronning Maud Land, Antarctica, Geol. Mag., 141, 1–12, 2004.

Engvik, A. K., Elvevold, S., Jacobs, J., Tveten, E., de Azevedo, S., and Njange, F.: Pan-African granulites of central Dronning Maud Land and Mozambique – a comparison within the East-African-Antarctic Orogen, in: A Keystone in a Changing World – Online Proceedings of the 10th ISAES, edited by: Cooper, A. K., Raymond, C. R., and the 10th ISAES Editorial Team, USGS Open-File Report 2007-1047, Short Research Paper 065, https://https://doi.org/10.3133/of2007-1047.srp065, 2007.

Faryad, S. W., Perraki, M., and Vrana, S.: P–T evolution and reaction textures in retrogressed eclogites from Svetlik, the Moldanubian Zone (Czech Republic), Miner. Petrol., 88, 297–319, 2006.

Franz, G. and Spear, F. S.: Aluminous titanite form the Eclogite Zone, south central Tauern Window, Austria, Chem. Geol., 50, 33–46, 1985.

Fraser, G., Ellis, D., and Eggins, S.: Zirconium abundance in granulite-facies minerals, with implications for zircon geochronology in high-grade rocks, Geology, 25, 607–610, 1997.

Frost, R. B. and Frost, C. D.: A geochemical classification for feldspathic igneous rocks, J. Petrol., 49, 1955–1969, https://doi.org/10.1093/petrology/egn054, 2008.

Godard, G. and Palmeri, R.: High-pressure metamorphism in Antarctica from the Proterozoic to the Cenozoic: A review and geodynamic implications, Gondwana Res., 23, 844–864, 2013.

Grantham, G. H., Jackson, C., Moyes, A. B., Groenewald, P. B., Harris, P. D., Ferrar, G., and Krynauw, J. R.: The tectonothermal evolution of the Kirwanveggen-Sverdrupfjella terrains, Dronning Maud Land, Antarctica, Precambrian Res., 75, 209–230, 1995.

Grew, E.S., Asami, M., and Makimoto, H.: Preliminary petrological studies of the metamorphic rocks of the eastern Sør Rondane Mountains, East Antarctica, Proceedings of the NIPR symposium on Antarctic geosciences, National Institute of Polar Research, Tokyo, Japan, 100–127, 1989.

Groenewald, P. B., Moyes, A. B., Grantham, G. H., and Krynauw, J. R.: East Antarctic crustal evolution: geological constraints and modelling in western Dronning Maud Land, Precambrian Res., 75, 231–250, 1995.

Hanson, R. E., Crowley, J. L., Bowring, S. A., Ramezani, J., Gose, W. A., Dalziel, I. W. D., Pancake, J. A., Seidel, E. K., Blenkinsop, T. G., and Mukwakwami, J.: Coeval large-scale magmatism in the Kalahari and Laurentian cratons during Rodinia assembly, Science, 304, 1126–1129, 2004.

Harlov, D., Tropper, P., Seifert, W., Nijland, T., and Hans-Jürgen Förster, H. J.: Formation of Al-rich titanite ($CaTiSiO_4O$–$CaAlSiO_4OH$) reaction rims on ilmenite in metamorphic rocks as a function of fH_2O and fO_2, Lithos, 88, 72–84, https://doi.org/10.1016/j.lithos.2005.08.005, 2006.

Hawthorne, F. C., Oberti, R., Harlow, G. E., Maresch, W. V., Martin, R. F., Schumacher, J. C., and Welch, M. D.: Nomenclature of the amphibole supergroup, Am. Mineral., 97, 2031–2048, https://doi.org/10.2138/am.2012.4276, 2012.

Hendriks, B. W. H., Engvik, A. K., and Elvevold, S.: $^{40}Ar/^{39}Ar$ record of late Pan-African exhumation of a granulite facies terrain, central Dronning Maud Land, East Antarctica, Miner. Petrol., 107, 665–677, https://doi.org/10.1007/s00710-012-0205-y, 2013.

Hiess, J., Condon, D. J., McLean, N., and Noble, S. R.: $^{238}U/^{235}U$ systematics in terrestrial uranium-bearing minerals, Science, 335, 1610–1614, 2012.

Hirajima, T., Zhang, R., and Cong, B.: Petrology of the nyböite-bearing eclogite in the Donghai area, Jiangsu Province, eastern China, Mineral. Mag., 56, 37–46, 1992.

Jackson, S. E., Pearson, N. J., Griffin, W. L., and Belousova, E .A.: The application of laser ablation-inductively coupled plasma-mass spectrometry to in situ U–Pb zircon geochronology, Chem. Geol., 211, 47–69, 2004.

Jacobs, J., Fanning, C. M., Henjes-Kunst, F., Olesch, M., and Paech, H.-J.: Continuation of the Mozambique Belt into East Antarctica: Grenville-Age Metamorphism and Polyphase Pan-African High-Grade Events in Central Dronning Maud Land, J. Geol., 106, 385–406, 1998.

Jacobs, J., Bauer, W., and Fanning, C. M.: New age constraints for Grenville-age metamorphism in western central Dronning Maud Land (East Antarctica), and implications for the paleogeography of Kalahari in Rodinia, Int. J. Earth Sci., 92, 301–315, 2003a.

Jacobs, J., Bauer, W., and Fanning, C. M.: Late Neoproterozoic/Early Paleozoic events in central Dronning Maud Land and significance for the southern extension of the East African Orogen into East Antarctica, Precambrian Res., 126, 27–53, 2003b.

Jacobs, J., Bingen, B., Thomas, R. J., Bauer, W., Wingate, M. T. D., and Feitio, P.: Early Paleoproterozoic orogenic collapse and voluminous late tectonic magmatism in Dronning Maud Land and Mozambique: insight into the partially delaminated orogenic root of the East African-Antarctic Orogen?, in: Geodynamic evolution of East Antarctica: a key to the East-West Gondwana connection, edited by: Satish-Kumar, M., Motoyoshi, Y., Osanai, Y., Hiroi, Y., and Shiraishi, K., Geol. Soc. Lond. Spec. Publ., 308, 69–90, 2008.

Jacobs, J., Elburg, M. A., Läufer, A., Kleinhanns, I. C., Henjes-Kunst, F., Estrada, S., Ruppel, A. S., Damaske, D., Montero, P., and Bea, F.: Two distinct Late Mesoproterozoic/Early Neoproterozoic basement provinces in central/eastern Dronning Maud Land, East Antarctica: The missing link, 15–21° E, Precambrian Res., 265, 249–272, https://doi.org/10.1016/j.precamres.2015.05.003, 2015.

Jacobs, J., Mikhalsky, E., Henjes-Kunst, F., Läufer, A., Thomas, R. J., Elburg, M. A., Wang, C. C., Estrada, and Skublov, S. G.: Neoproterozoic geodynamic evolution of easternmost Kalahari: Constraints from U-Pb-Hf-O zircon, Sm-Nd isotope and geochemical data from the Schirmacher Oasis, East Antarctica, Precambrian Res., 342, 105553, https://doi.org/10.1016/j.precamres.2019.105553, 2020.

Joanny, V., Van Roermund, H., and Lardeaux, J. M.: The clinopyroxene plagioclase symplectite in retrograde eclogites – A Potential geothermobarometer, Geol. Rundsch., 80, 303–320, 1991.

Kennedy, W. Q.: The structural differentiation of African in the Pan-African (± 500 m.y.) tectonic episode, 8th Annual Report of the Research Institute of African Geology, University of Leeds, UK, 48–49, 1964.

Kohn, M. J., Corrie S. L., and Markley, C.: The fall and rise of metamorphic zircon, Am. Mineral., 100, 897–908, 2015.

Koon, P. O. and Thompson, A. B.: Non-mafic rocks in the greenschist, blueschist and eclogite facies, Chem. Geol., 50, 3–30, https://doi.org/10.1016/0009-2541(85)90109-3, 1985.

Krogh, E. J., Andresen, A., Bryhni, I., Broks, T. M, and Kristensen, S. E.: Eclogites and polyphase *P-T* cycling in the Caledonian Uppermost Allochthon in Troms, northern Norway, J. Metamorph. Geol., 8, 289–309, 1990.

Marsh, J. K. and Kelly, E. D.: Petrogenetic relations among titanium-rich minerals in an anatectic high-P mafic granulite, J. Metamorph. Geol., 35, 717–738, 2017.

McDonough, W. F. and Sun, S.-S.: The composition of the Earth, Chem. Geol., 120, 223–253, 1995.

Mikhalsky, E. V., Beliatsky, B. V., Savva, E. V., Wetzel, H.-U., Fedorov, L. V., Weiser, T., and Hahne, K.: Reconnaissance geochronological data on polymetamorphic and igneous rocks of the Humboldt Mountains, central Queen Maud Land, East Antarctica, in: The Antarctic Region: Geological Evolution and Processes, edited by: Ricci, C. A., Terra Antarctica Publication, Siena, 45–53, ISBN 88-900221-0-8, 1997.

O'Brien, P. J. and Rötzler, J.: HP granulites: formation, recovery of peak conditions and implications for tectonics, J. Metamorph. Geol., 21, 3–20, 2003.

Oh, C. W. and Liou, J. G.: A petrogenetic grid for eclogite and related facies under high-pressure metamorphism, Isl. Arc, 7, 36–51, 1998.

Palmeri, R., Godard, G., Di Vincenzo, G., Sandroni, S., and Talarico, F. M.: High-pressure granulite-facies metamorphism in central Dronning Maud Land (East Antarctica): Implications for Gondwana assembly, Lithos, 300/301, 361–377, https://doi.org/10.1016/j.lithos.2017.12.014, 2018.

Passchier, C. W. and Trouw, R. A. J.: Microtectonics, Springer, 2nd Edn. 205, ISBN 978-3-540-64003-5, ISBN 3-540-58713-6, 1998.

Paton, C., Woodhead, J. D., Hellstrom, J. C., Hergt, J. M., Greig, A., and Maas, R.: Improved laser ablation U-Pb zircon geochronology through robust downhole fractionation correction, Geochem. Geophy. Geosy., 11, Q0AA06, https://doi.org/10.1029/2009GC002618, 2010.

Paton, C., Hellstrom, J., Paul, B., Woodhead, J., and Hergt, J.: Iolite: Freeware for the visualisation and processing of mass spectrometric data, J. Anal. Atom. Spectrom., 26, 2508–2518, 2011.

Paulsson, O. and Austrheim, H.: A geochronological and geochemical study of rocks from the Gjelsvikfjella, Dronning Maud Land, Antarctica – implications for Mesoproterozoic correlations and assembly of Gondwana, Precambrian Res., 125, 113–138, 2003.

Pauly, J., Marschall, H. R., Meyer, H. P., Chatterjee, N., and Monteleone, B.: Prolonged Ediacaran-Cambrian metamorphic history and short-lived HP granulite-facies metamorphism in the H.U. Sverdrupfjella, Dronning Maud Land (East Antarctica): Evidence for continental collision during Gondwana assembly, J. Petrol., 57, 185–228, 2016.

Pouchou, J. L. and Pichoir, F.: Cameca PAP program, La Recherche Aerospatiale, 3, 167–192, 1984.

Proyer, A.: The preservation of high-pressure rocks during exhumation: metagranites and metapelites, Lithos, 70, 183–194, 2003.

Rickwood, P. C.: Boundary lines within petrologic diagrams which use oxides of major and minor elements, Lithos 22, 247–263, 1989.

Riedel, S., Jacobs, J., and Jokat, W.: Interpretation of new regional aeromagnetic data over Dronning Maud Land (East Antarctica), Tectonophysics, 585, 161–171, https://doi.org/10.1016/j.tecto.2012.10.011, 2013.

Rubatto, D.: Zircon: The metamorphic mineral. Reviews in Mineralogy and Geochemistry, 83, 261–295, https://doi.org/10.2138/rmg.2017.83.9, 2017.

Sartini-Rideout, C., Gilotti, J. A., and Foster, C. T.: Forward modeling corona growth in a partially eclogitized leucogabbro, Bourbon Island, North-East Greenland, Lithos, 95, 279–297, 2007.

Schmädicke, E. and Will, T. M.: First evidence of eclogite facies metamorphism in the Shackleton Range, Antarctica; trace of a suture between east and west Gondwana?, https://doi.org/10.1130/G22170.1, 2006.

Sláma, J., Košler, J., Condon, D. J., Crowley, J. L., Gerdes, A., Hanchar, J. M., Horstwood, M. S. A., Morris, G. A., Nasdala, L., Norberg, N., Schaltegger, U., Schoene, B., Tubrett, M. N., and Whitehouse, M. J.: Plešovice zircon – a new natural reference material for U–Pb and Hf isotopic microanalysis, Chem. Geol., 249, 1–35, 2008.

Smith, D. C.: Highly aluminous sphene (titanite) in natural HP hydrous-eclogite facies rocks from Norway to Italy, and in experimental runs at high pressure, Abstract, 26th International Geological Congress, Paris, 1980.

Sun, S.-S. and McDonough, W. F.: Chemical and isotopic systematics of oceanic basalts: implications for mantle composition and processes, Geol. Soc. Lond. Spec. Publ., 42, 313–345, https://doi.org/10.1144/GSL.SP.1989.042.01.19, 1989.

Thompson, A. B. and Connolly, J. A. D.: Melting of the continental crust: Some thermal and petrological constraints on anatexis in continental collision zones and other tectonic settings, J. Geophys. Res., 100, 15565–15579, 1995.

Troitzsch, U. and Ellis, D. J.: The synthesis and crystal structure of CaAlFSiO4, the Al-F analog of titanite, Am. Mineral., 84, 1162–1169, 1999.

Troitzsch, U. and Ellis, D. J.: Thermodynamic properties and stability of AlF-bearing titanite $CaTiOSiO_4$-$CaAlFSiO_4$, Contrib. Mineral. Petr., 142, 543–563, 2002.

Vermeesch, P.: IsoplotR: A free and open toolbox for geochronology, Geosci. Front., 9, 1479–1493, 2018.

Wang, C.-C., Jacobs, J., Elburg, M. A., Läufer, A., and Elvevold, S.: Late Neoproterozoic-Cambrian magmatism in Dronning Maud Land (East Antarctica): U-Pb zircon geochronology, isotope geochemistry and implications for Gondwana assembly, Precambrian Res., 350, 105880, https://doi.org/10.1016/j.precamres.2020.105880, 2020a.

Wang, C.-C., Jacobs, J., Elburg, M. A., Läufer, A., Thomas, R. J., and Elvevold, S.: Grenville-age continental arc magmatism and crustal evolution in central Dronning Maud Land (East Antarctica): Zircon geochronological and Hf-O isotopic evidence, Gondwana Res., 82, 108–127, https://doi.org/10.1016/j.gr.2019.12.004, 2020b.

Whitney, D. L., and Evans, B. W.: Abbreviations of names of rock-forming minerals, Am. Mineral, 95, 185–187, 2010.

Wiedenbeck, M. A. P. C., Alle, P., Corfu, F. Y., Griffin, W. L., Meier, M., Oberli, F. V., Von Quadt, A., Roddick, J. C., and Spiegel, W.: Three natural zircon standards for U-Th-Pb, Lu-Hf, trace element and REE analyses, Geostandard Newslett., 19, 1–23, 1995.

Yakymchuk, C., Clark, C., and White, R. W.: Phase relations, reaction sequences and petrochronology, in: Petrochronology: Methods and Applications, edited by: Kohn, M. J., Engi, M., and Lanari, P., Rev. Mineral. Geochem., 13–53, https://doi.org/10.2138/rmg.2017.83.2, 2017.